Available online at www.sciencedirect.com
SCIENCE DIRECT®
Journal of Nuclear Materials 323 (2003) 41–48
journal of nuclear materials
www.elsevier.com/locate/jnucmat

Characterization of zirconia–thoria–urania ceramics by X-ray and electron interactions

Gini Curran [a], Y. Sevestre [a,b], Wendy Rattray [a], Patrick Allen [c], K.R. Czerwinski [a,*]

[a] *Actinide Research Group, Department of Nuclear Engineering, Massachusetts Institute of Technology, NW13-219, 77 Massachusetts Avenue, Cambridge, MA 02139, USA*
[b] *Ecole Nationale Supérieure de Chimie de Paris, 11, rue Pierre et Marie Curie, 75005 Paris, France*
[c] *Glenn Seaborg Institute, Lawrence Livermore National Laboratory, 7000 East Avenue, P.O. Box 808, L-231, Livermore, CA 94511 USA*

Received 30 January 2003; accepted 31 July 2003

Abstract

X-ray and electron interactions with matter were used as probes to characterize the structure and chemistry of zirconia–thoria–urania ceramics. The ceramics were prepared by coprecipitation of Zr, Th and U salts. In this study, transmission electron microscopy (TEM) techniques such as energy dispersive X-ray (EDX) analysis and electron energy loss spectroscopy (EELS) complement X-ray diffraction, extended X-ray absorption fine structure (EXAFS) and X-ray absorption near edge spectroscopy (XANES), techniques to reveal the phase structure and chemistry. The results from XRD and EDX show that these ceramics separate into a Zr-based phase and an actinide-based phase with low mutual affinity of Th and Zr, as well as partial solubility of U in Zr. The comparison of EELS spectra collected for the ceramics with spectra collected for UO_2 and U_3O_8 reference materials also allow us to assess U oxidation state independently in the two separate phases.

PACS: 61.66.Fn; 61.10.Nz; 61.16.Yc

1. Introduction

There has been a recent resurgence of interest in Th as a potential fuel for generation IV nuclear reactors. It is thought that ThO_2–UO_2 will be less expensive to fabricate than standard UO_2 fuel, result in a more stable and insoluble waste form, and be resistant to weapons-material proliferation [1]. The intent of this work is to synthesize and characterize a series of ThO_2–UO_2 ceramics with varied amounts of ZrO_2. The ratio of Th to U is held at three based on reactor physics considerations. The overall metal stoichiometry is Zr_xTh_3U with $x = 0$, 1, 3 and 6. While this work examines a range of relative Zr concentration, in the case of a realistic fuel only the lowest Zr concentrations can be considered. The characterization will reveal the speciation of the actinides in the ceramics and the information will be used in the further analysis of actinide solubility.

The addition of ZrO_2 in the ceramic material is based on the expected enhancement in chemical stability and radiation resistance [2]. The natural analogue of zirconia, baddeleyite ($(Zr,M)O_2$), where M is a tetravalent ion such as hafnium, contains up to 3000 ppm U or Th [3]. Negligible or no lead loss (a stable decay product of U and Th) in natural baddeleyites indicates high long-term chemical durability of the material in the environment [3]. Studies have shown that zirconia is more radiation resistant than both pyrochlore ($Gd_2Ti_2O_7$) and zirconalite ($CaZrTi_2O_7$) ceramics [2,4].

* Corresponding author. Tel.: +1-617 253 3843; fax: +1-617 253 7300.
E-mail address: kczer@mit.edu (K.R. Czerwinski).

0022-3115/$ - see front matter © 2003 Elsevier B.V. All rights reserved.
doi:10.1016/j.jnucmat.2003.07.005

There has been previous work on the fabrication and characterization of UO_2–ThO_2 ceramics [5,6]. Various zirconia-containing ceramics have been fabricated and studied, including ZrO_2–PuO_2, ZrO_2–UO_2, ZrO_2–Gd_2O_3–PuO_2, ZrO_2–Y_2O_3–NpO_2, ZrO_2–ThO_2 and ZrO_2–CeO_2 [2,7–12]. Ceramics that have been fabricated frequently contain a Y_2O_3 (up to 15 mol.% [2]) binder in order to stabilize the ceramic. Though there have been problems with urania–thoria phase separation, the inclusion of Zr in the lattice tends to strengthen the bonding [5], and all of these ceramic compositions have shown superior durability to their zirconia-free counterparts [2,4–6].

Uranium and thorium dioxide have the same fluorite structure with similar lattice constants, 5.468 and 5.59 Å respectively. They form perfect solid solutions with a fluorite structure and a cell parameter characteristic of the phase composition. The unit-cell parameter of the solid solutions follows almost exactly a straight-line relation with composition [13]. For the UO_2–ZrO_2 and ThO_2–ZrO_2 systems, two solid solutions are formed: $(ZrO_2)_{SS}$ and $(MO_2)_{SS}$, where M=U or Th. There is little mutual solubility of the actinides in ZrO_2 under the conditions examined [13,14]. While there is a fairly diverse array of data on the behavior of thoria, urania and zirconia, no studies of a combined ZrO_2–ThO_2–UO_2 system have been published.

This study focuses mainly on establishing the phase structure and composition of selected zirconia–thoria–urania ceramic systems. In addition, the oxidation state of U is known to be one of the key factors controlling U solubility. Therefore, the U oxidation state in the ceramics is characterized. The ceramics are used in solubility experiments to thermodynamically and kinetically evaluate the component material dissolution and acquired data for modeling the repository behavior of the ceramics [15].

2. Experimental

2.1. Ceramic preparation

Computer simulations showed that a 3:1 Th:U ratio offered the best compromise for nuclear fuel applications [1]. This ratio will therefore remain constant for this study and only the Zr content will be varied to determine the ideal composition relative to nuclear waste form stability. The ceramics under investigation have a constant Th:U ratio of 3:1 and an overall metal ratio of Zr_xTh_3U with $x = 0$, 1, 3 and 6. Simple compositions of Zr:Th and Zr:U binary systems were also synthesized for this study.

The ceramics were fabricated from a solution of uranyl nitrate ($UO_2(NO_3)_2 \cdot 6H_2O$), thorium nitrate ($Th(NO_3)_4 \cdot 4H_2O$) and zirconyl chloride ($ZrOCl_2 \cdot 8H_2O$) dissolved in purified water. The Zr, Th and U were slowly coprecipitated out of solution in a mixture of oxalic acid and an excess of NH_4OH. Once the precipitate settled, the excess liquid was drained and the precipitate was washed, twice with purified water and twice with acetone. This yielded a mixture of oxalates and hydroxides. The final washed precipitate was then placed in an oven at 90 °C to dry overnight. After the first drying period, the precipitate is removed from the oven and ground in a porcelain mortar to a homogenous powder. The powder was then further dried at 150 °C for several hours, calcined at 700 °C for one hour and then cold pressed in a 13 or 7 mm cylindrical die at 55 MPa for 2 min. The resulting pellets were sintered at 1500 °C under a $3\%H_2/1\%O_2/96\%Ar$ atmosphere for 4 h in order to reduce the U from U(VI) to U(IV). For some samples, 0.5 wt% magnesium oxide was added to the powder after the calcination step as a binder in order to increase the ceramics density and strength.

2.2. Sample characterization

2.2.1. Transmission electron microscopy

The synthesized ceramic materials were prepared for Transmission electron microscopy (TEM) analysis by mechanical polishing and ion milling with an incident angle of 15°. The analysis was carried out on a JEOL 200 TEM and was mainly focused on the grain structure of the ceramics, the average grain size being measured on negative films.

2.2.2. Energy dispersive X-ray and electron energy loss spectroscopy

The ceramic samples prepared for TEM were also evaluated by energy dispersive X-ray (EDX) and electron energy loss spectroscopy (EELS). The samples were coated with a 200 Å conductive carbon layer in order to avoid electrostatic charging of the material. The UO_2 and U_3O_8 reference samples for EELS were prepared by embedding standard powdered materials, from Alfa Aesar and NBL respectively, in epoxy resin and thin sectioning the resin blocks. The sections produced by this technique were laid on 200 mesh copper grids and carbon coated. A ThO_2 sample was also prepared the same way, using precipitated and calcined powder. The EDX and EELS analyses were carried out on a VG HB603 scanning transmission electron microscope operated at 250 kV with a field emission gun that was equipped with a large collection-angle X-ray detector and a parallel EELS spectrometer. The integration time for EELS analysis was 8 s, and 10–25 readouts were accumulated for each spectrum depending on the sample thickness. Data was collected at 0.5 eV/Channel using ELP software. The edges in the EELS spectra for the various phases present in the ceramic samples were identified by comparison with the spectra collected from

the reference materials. Slight energy shifts were observed due to gun voltage fluctuations throughout the experiment, but they should have no influence on the edge shapes. ORIGIN software was used to correct the baseline of EELS spectra and to calculate the peak area for U M_4 and M_5 edges.

The EELS technique has close similarities with the corresponding X-ray absorption spectroscopy (XAS) technique and can be used to evaluate the oxidation state of elements. More specifically, the two intense features on the M_4 and M_5 edges of the actinides correspond to the two electronic transitions $3d_{3/2} \rightarrow 5f_{5/2}$ and $3d_{5/2} \rightarrow 5f_{7/2}$, respectively, that arise from the spin-orbit splitting [16]. In the case of rare earths, the M_4/M_5 ratio is observed to decrease with increasing 4f orbital occupancy [17] and the M_4/M_5 ratio obtained with EELS has been used to determine the oxidation state for rare-earth elements [18]. Although it is tempting to extrapolate from the 4f chemistry to deduce the behavior for the 5f elements, no data has been published so far in this area and caution must be used as the itinerant nature of the 5f orbitals leads to strong hybridization with the 6d and 7s orbitals [19]. In this study, the spectra collected for the various ZrO_2–ThO_2–UO_2 systems will be compared to UO_2 and U_3O_8 reference sample spectra, focusing on the M_4/M_5 ratio to assess the oxidation state of uranium in the ceramics. This data will be compared with the XAS technique to validate the oxidation state analysis.

2.2.3. X-ray diffraction

For X-ray powder diffraction the ceramic pellets were ground into a powder, mixed with 1/3 collodion/amyl acetate solution and 2–3 mg of 640 c silicon standard from NIST used as an internal reference for peak calibration. The analysis was performed using a Rigaku 300 diffractometer and CuKα radiation. Phase characterization was completed using Jade software and lattice parameters were determined by performing a least square regression on the 2θ-values for the 10 most intense peaks on the calibrated patterns.

2.2.4. X-ray absorption spectroscopy

Preparation for XAS analysis consisted of grinding each sintered pellet into a fine powder. Approximately 50 mg of powder from each pellet was mixed with 200 mg BioBeads and sealed in an aluminum window with Kapton tape. Several transmission spectra were taken for each sample. Samples were scanned over the Th and U L_3-edges and the Zr K-edge. Simultaneously measured UO_2 standard, Zr metal standard, and Th_3UO_8 sample were used for calibration of the absorption edge. extended X-ray absorption fine structure (EXAFS) and X-ray absorption near edge spectroscopy (XANES) data was collected at the Stanford Synchrotron Radiation Laboratory (SSRL). Raw data treatment and analysis was performed using standard methods reviewed elsewhere [20,21] using EXAFSPAK, developed by George of SSRL. Autobk [22] was used to fit μ_o(E) using a piecewise spline for the U and Zr data. Phase and amplitude functions were calculated using FEFF8.1 developed by Rehr et al. [23,24].

3. Results and discussion

3.1. Density

After sintering, the diameter and thickness of each pellet was measured and weighed to determine the ceramic density. Inclusion of Zr in the ceramics decreases density, while the addition of magnesium oxide increases ceramic density from 5% to 20%, the effect of magnesium oxide increasing with increased Zr content. The average grain size of the ceramics varies from 0.4 to 0.8 μm.

3.2. Spectroscopic analysis

3.2.1. X-ray diffraction results

The results of XRD analysis are presented in Table 1. The analysis of the binary systems reveals mutual affinities between the various species. As expected from previous studies, U and Th show perfect solubility. When UO_2 and ZrO_2 are sintered together, a metastable Zr-based tetragonal phase is formed, revealing solubility of U in Zr, contrary to the case of Th and Zr where two thermodynamically stable phases form. The phase structure of the ternary ZrO_2–ThO_2–UO_2 systems is clearly established. Regardless of the Zr content, a ThO_2–UO_2 solid solution with a cubic fluorite structure forms that is separate from a ZrO_2 based phase. The ZrO_2 phase contains UO_2 and MgO. In the case of UO_2–ThO_2 solid solutions, the U/Th ratio is determined by assuming a straight-line relation between the cell parameter and the phase composition using Jade reference data (Table 2). The variation in the specific Th:U ratio for the solid solutions is due to the formation of a separate Zr–U phase.

3.2.2. Energy dispersive X-ray results

In the EDX elemental mappings (Figs. 1 and 2), two separate phases clearly appear for all the ternary systems. One phase shows a high Th concentration and the other a high Zr concentration. This confirms the previous XRD results and that the mutual solubility of Zr and Th are low. Uranium is present in both Zr and Th phases in significant levels. Magnesium is homogenously distributed throughout the ceramics. The key result of this analysis is that the synthesis method provides good homogenous composition of the starting material and the phase separation occurs during the sintering phase.

Table 1
Phase characterization of standards and samples by XRD

Standards	Major phases	XRD matching structures	Reference Jade PDF #
ZrO_2	1	ZrO_2 (baddeleyite)	37-1484
$ZrThO_4$	2	ThO_2	42-1462
		ZrO_2 (baddeleyite)	37-1484
$ZrUO_4$	1	ZrO_2 (tetragonal)	42-1164
$ZrUO_4$	2	U_3O_8	31-1424
		ZrO_2 (tetragonal)	17-0923
Samples (metal ratio)			
Th_3UO_8	1	$(ThO_2)0.75$–$(UO_2)0.25$	30-1360
$ZrTh_3U$	2	$(ThO_2)0.5$–$(UO_2)0.5$	33-1368
		ZrO_2 (cubic)	20-0684
$ZrTh_3U + Mg$	2	$(ThO_2)0.5$–$(UO_2)0.5$	33-1368
		ZrO_2 (tetragonal)	42-1164
Zr_3Th_3U	2	$(ThO_2)0.75$–$(UO_2)0.25$	30-1360
		ZrO_2 (cubic)	27-0997
$Zr_3Th_3U + Mg$	2	$(ThO_2)0.75$–$(UO_2)0.25$	30-1360
		ZrO_2 (baddeleyite)	37-1484
Zr_6Th_3U	2	$(ThO_2)0.5$–$(UO_2)0.5$	33-1368
		ZrO_2 (baddeleyite)	37-1484
$Zr_6Th_3U + Mg$	2	$(ThO_2)0.5$–$(UO_2)0.5$	33-1368
		ZrO_2 (baddeleyite)	37-1484

Table 2
ThO_2–UO_2 solid solution compositions and cell parameter from XRD analysis

Sample metal ratio	Cell parameter (Å)	Th–U composition
PDF database Ref 33-1368	5.530	$Th_{0.5}U_{0.5}O_2$
PDF database Ref 30-1360	5.559	$Th_{0.75}U_{0.25}O_2$
Zr_6Th_3U	5.552 ± 0.010	$Th_{0.69}U_{0.31}O_2$
Zr_6Th_3U	5.551 ± 0.007	$Th_{0.68}U_{0.32}O_2$
$Zr_6Th_3U + Mg$	5.551 ± 0.006	$Th_{0.68}U_{0.32}O_2$
Zr_3Th_3U	5.554 ± 0.006	$Th_{0.71}U_{0.29}O_2$
$Zr_3Th_3U + Mg$	5.565 ± 0.007	$Th_{0.8}U_{0.2}O_2$
$ZrTh_3U$	5.521 ± 0.005	$Th_{0.42}U_{0.58}O_2$
$ZrTh_3U + Mg$	5.524 ± 0.006	$Th_{0.45}U_{0.55}O_2$
Th_3U	5.559 ± 0.003	$Th_{0.75}U_{0.25}O_2$

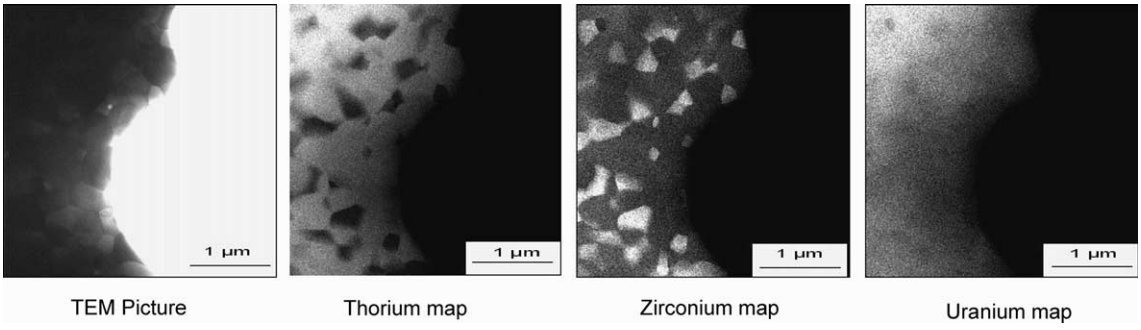

Fig. 1. EDX elemental map of ceramic with $ZrTh_3U$ metal ratio. The elements under consideration appear bright. Thorium and zirconium maps appear as negatives of each other, showing low mutual solubility of these two elements. Uranium is homogenously distributed throughout the ceramic.

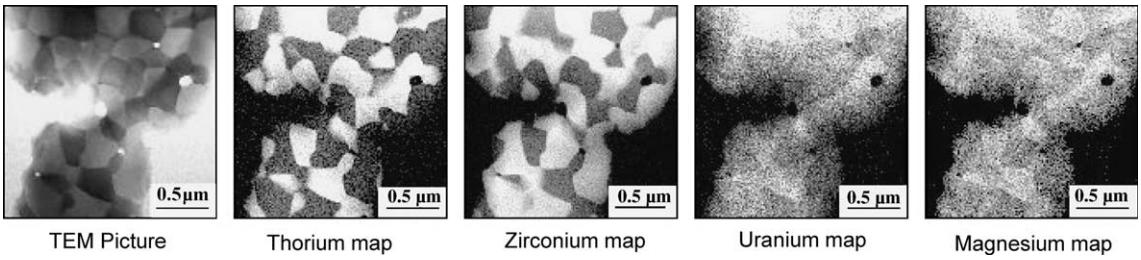

Fig. 2. EDX elemental map of Zr_6Th_3U metal ratio + 0.5 wt% MgO. Thorium and zirconium separate in two different phases. Uranium and magnesium are homogenously distributed throughout the sample.

3.2.3. Electron energy loss spectroscopy results

The EELS spectra were collected for each UO_2 and U_3O_8 reference samples on the thin areas of different grains (Fig. 3). For the ceramic samples, the spectra from the Th rich phase are easily recognizable from the spectra of the low Th phase as the Th edges are less intense than the U edges. This result confirms the EDX observations. The average M_4/M_5 ratios were calculated for the standards and the samples (Table 3). Differences between the UO_2 and U_3O_8 ratio values are observed and the oxidation state of U samples can be determined with this method. The results show oxidation of U is found in the Zr phase.

Table 3
M_4/M_5 ratio for U in standards and samples

Standards	M_4/M_5
UO_2	0.41 ± 0.03
U_3O_8	0.48 ± 0.03
Samples (metal ratio and phase)	
Th_3U	0.40 ± 0.04
$ZrTh_3U$ (Th phase)	0.41 ± 0.04
$ZrTh_3U$ (Zr phase)	0.46 ± 0.07
Zr_3Th_3U (Th phase)	0.43 ± 0.06
Zr_3Th_3U (Zr phase)	0.45 ± 0.06
Zr_6Th_3U (Th phase)	0.45 ± 0.08
Zr_6Th_3U (Zr phase)	0.51 ± 0.12

3.2.4. XANES spectra

Thorium spectra were scanned on the Th L_3-edge to $k = 13$ in order to avoid the U pre-edge. Thorium XANES spectra were consistent with ThO_2, as expected for the Th(IV) environment. The Zr K edge was scanned to $k = 14$ revealing some fine structure in the pre-edge. The U L_3 edge was scanned to $k = 14$ and the peaks

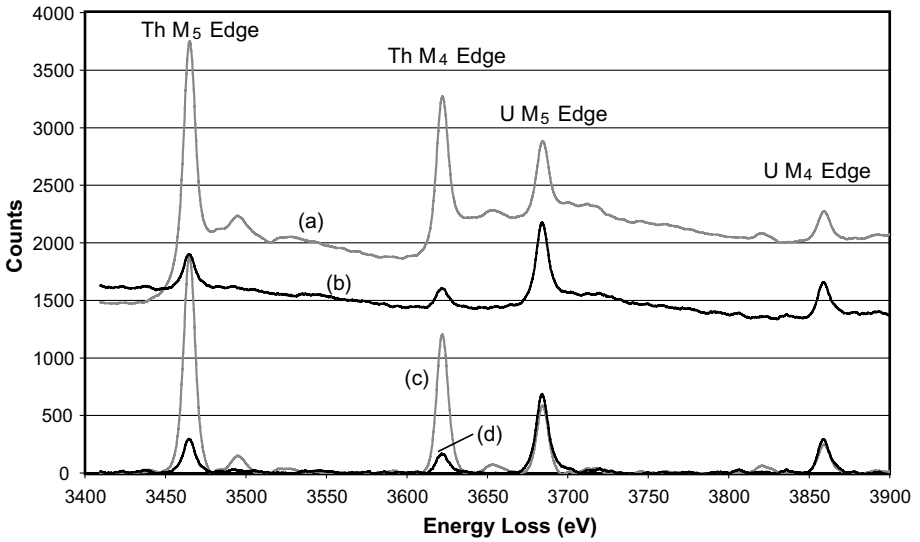

Fig. 3. EELS spectra of ceramic samples. (a) Th_3UO_8 raw data, (b) $ZrTh_3UO_{10}$ low thorium phase, (c) baseline correction of spectrum (a), (d) baseline correction of spectrum (b). In low thorium phases (spectra b, d) thorium edges are less intense than the corresponding uranium edges.

appear to shift to the right with higher zirconia content. The U XANES spectra lack the characteristic shoulder indicative of uranyl, and appear shifted to higher energies than the UO_2 standard, indicating an intermediate oxidation state (Fig. 4). The spectra shift to higher energies as the zirconium content increases.

3.2.5. EXAFS results

Average bond lengths and coordination numbers from the EXAFS analysis are given in Table 4. The Fourier transforms of the Th data confirm the structural similarities to ThO_2. Uranium and Th are completely interchangeable in the Th oxide lattice. Analysis of the U Fourier transforms (Fig. 5) showed that all samples exhibited contracted U–O bond lengths when compared to the UO_2 reference. Contraction increased with increasing Zr content, verifying the increasing oxidation of U with Zr content observed by EELS and XANES. Analysis of the Zr spectra for each sample showed that the average Zr–M bond length decreased with increasing Zr content. The addition of 0.5 wt% MgO decreased the average Zr–M bond length for the $ZrTh_3U$ sample, but had no noticeable effect on the higher Zr content samples. This shortened average bond length appeared to effect the amount of U in the zirconia lattice. Curve fitting of the $ZrTh_3U$ samples with and without MgO showed that the samples with no MgO fit best with a U placed at the second position, while those with Mg fit best with a Zr at that position (Figs. 6 and 7).

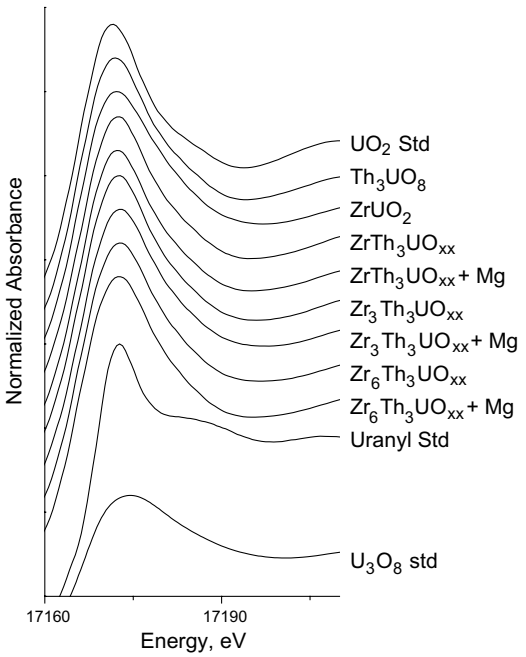

Fig. 4. Uranium L_3 XANES spectra for the uranium standards and samples.

Table 4
Bond lengths and coordination numbers for Zr and U in the ceramic samples measured by EXAFS

Sample	Bond	N	R (Å)
Th_3U	Th–O	8	2.40
Th_3U	Th–(U, Th)	12	3.94
Th_3U	U–O	8	2.28
Th_3U	U–(Th, U)	12	3.92
$ZrTh_3U$	U–O	4.2	2.26
$ZrTh_3U$	U–(Zr, Th, U)	2.6	3.91
$ZrTh_3U$	Zr–(Zr, Th, U)	12	3.71
Zr_3Th_3U	U–O	3.2	2.19
Zr_3Th_3U	U–(Th, U)	2.7	3.76
Zr_3Th_3U	Zr–(Zr, Th, U)	12	3.56

Th values are averaged over all samples. The samples are defined by the metal ratio. The error in the bond lengths are 3%.

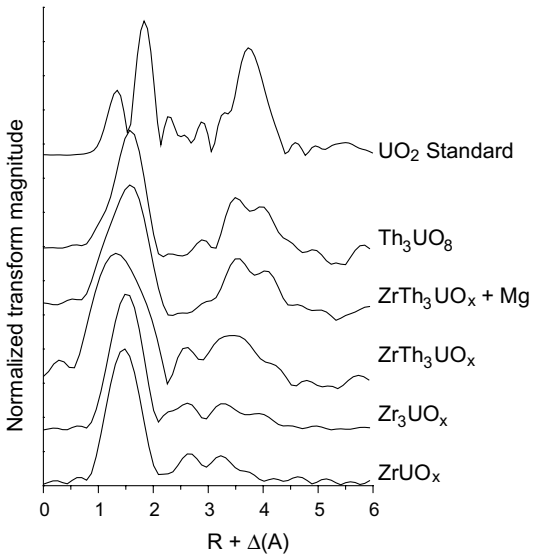

Fig. 5. Uranium EXAFS Fourier transforms.

4. Conclusions

The mutual affinities in ZrO_2–ThO_2–UO_2 systems are very similar to the ones observed in binary systems. Uranium, which has a good affinity with both Th and Zr is homogenously distributed throughout the ceramics, whereas Th and Zr form separate phases. Magnesium oxide, which is also soluble in both phases, increases the density of the material. The presence of Zr leads to oxidation of the U in the Zr rich phase, while Th helped stabilize the tetravalent form of U under the atmospheric conditions used in the sintering. This can be attributed to the strong chemical and physical similarity of tetravalent U with Th when compared to Zr. The actinides have similar electronic structures and ionic radii.

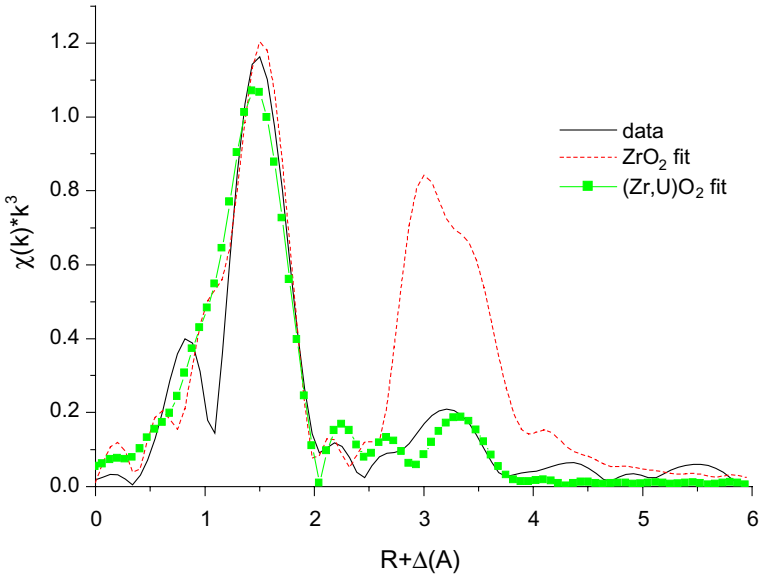

Fig. 6. EXAFS data and calculated fit for ceramics with a metal ratio of $ZrTh_3U$.

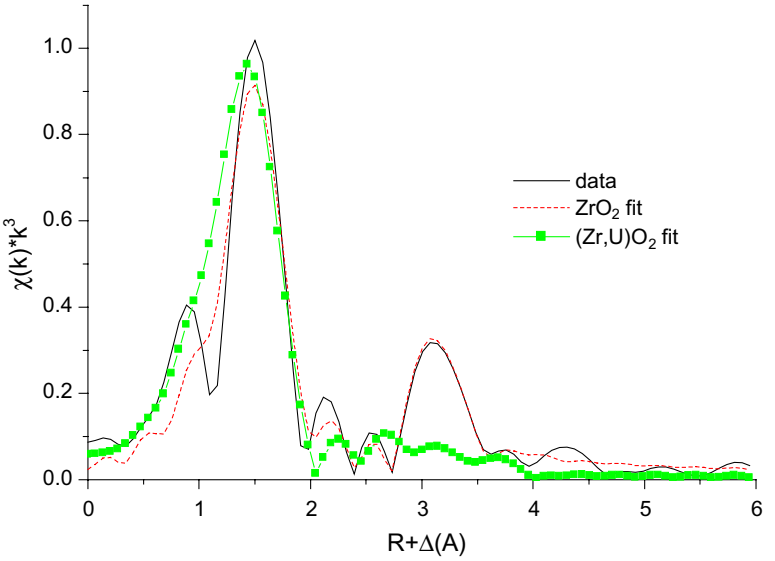

Fig. 7. EXAFS data and calculated fit for ceramics with a metal ratio of $ZrTh_3U + 5$ wt% MgO.

The EELS results show the method can be applied to the actinides, similar to previous investigations with the lanthanides. Extrapolating from the rare-earth chemistry and the previous results [17], we can assume that the M_4/M_5 ratio for 5f elements decreases with increasing 5f orbital occupancy, which is to say with decreasing oxidation state. For the actinides a large relative error in the M_4/M_5 ratio is expected. Since the energy of the 5f, 6d, 7s and 7p orbitals are comparable, there is considerable flexibility in electron configurations for a given oxidation state. However, a trend is confirmed by the M_4/M_5 analysis of U_3O_8 (U oxidation state = 5.3) and UO_2 (U oxidation state = 4) reference samples and is used to qualitatively assess the oxidation state of U in the different phases of the ceramic samples with results confirmed by other spectroscopic techniques.

Acknowledgements

The XRD and electron microscopy work was carried out at the Center for Materials Science and Engineering

at M.I.T. We thank Gordon Kohse, Professor Lynn Hobbs and Michael Frongillo for advice and help with sample preparation and Dr Garratt-Reed for help with EDX analysis and EELS data collection. Part of this work was performed under the auspices of the U.S. Department of Energy (DOE) by the University of California Lawrence Livermore National Laboratory under Contract No. W-7405-Eng-48. This work was done (partially) at Stanford Synchrotron Radiation Laboratory, which is operated by the Department of Energy, Division of Chemical Sciences.

References

[1] M. Kazimi et al. Advanced Proliferation Resistant, Lower cost, Uranium–Thorium Dioxide Fuels for Light Water Reactors, Nuclear Energy Research Initiative Project 99-0153 Quarterly Report, May 2000.
[2] W.L. Gong, W. Lutze, R.C. Ewing, J. Nucl. Mater 277 (2000) 239.
[3] M. Benedict, T.H. Pigford, H.V. Levi, Nuclear Chemical Engineering, 2nd Ed., McGraw-Hill, USA, 1981, p. 318.
[4] C.L. Crawford, C.R. Biddle, N.E. Bibler, Durability testing of heavy-ion irradiated.crystalline ceramics, Report, WSRC-MS-2000-00309. Avilable from <http://www.srs.gov/general/sci-tech/fulltext/ms2000309/ms2000309.html>.
[5] N.B. De Lima, K. Imakuma, J. Nucl. Mater 135 (1985) 215.
[6] V. Balek, J. Nucl. Mater 153 (1988) 41.
[7] E.B. Anderson, E.B. Burakov, V.G. Vasiliev, in: Proceedings of International Conference SAFE WASTE-93, 13–18 June 1993, Avignon, France, vol. 2, 1993, p. 29.
[8] K.-I. Kuramoto, Y. Makino, T. Yanagi, S. Muraoka, Y. Ito, in: Proceedings of the International Conference Global-95, 11–14 September 1995, Versailles, France, 1995, p. 1838.
[9] H. Kinoshita, K. Kuramoto, M. Uno, S. Yamanaka, H. Mitamura, T. Banba, in: Proceedings of the 2nd NUCEF International Symposium NUCEF'98, 16–17 November 1998, Hitachinaka, Ibaraki, Japan, JAERI-Conf.99-004 (Part I), 1998, p. 307.
[10] B.E. Burakov, E.B. Anderson, in: Proceedings of the 2nd NUCEF International Symposium NUCEF'98, 16–17 November 1998, Hitachinaka, Ibaraki, Japan, JAERI-Conf.99-004 (Part I), 1998, p. 295.
[11] B.E. Burakov, E.B. Anderson, in: Proceedings of the Meeting for Coordination and Review of Work, 1–4 November 1999, St. Petersburg, Russia, 2000, p. 167.
[12] B. Burakov, E. Anderson, Proceedings of the Meeting for Coordination and Review of Work, 13–16 November 2000, St. Petersburg, Russia, UCRL-ID-143846, 2001, p. 229.
[13] F.A. Mumpton, R. Rustum, J. Am. Ceram. Soc. 43 (1960) 237.
[14] J. Cohen, B.E. Schaner, J. Nucl. Mater. 9 (1963) 18.
[15] G. Curran, W. Rattray, K.R. Czerwinski, Radiochim. Acta 91 (2003) 203.
[16] E.C. Buck, J.A. Fortner, Ultramicroscopy 67 (1997) 69.
[17] B.T. Hole, G. Van der Laan, J.C. Fuggle, G.A. Swatzky, R.C. Karnatak, J.-M. Esteva, Phys. Rev. B 32 (1985) 5107.
[18] J.A. Fortner, E.C. Buck, Appl. Phys. Lett. 68 (1996) 3817.
[19] P.W. Atkins, Eur. J. Sol. State Inorg. Chem. 28 (1991) 9.
[20] T.M. Hayes, J.B. Boyce, Solid State Phys. 37 (1982) 173.
[21] G.G. Li, F. Bridges, C.H. Booth, Phys. Rev. B 52 (1995) 6332.
[22] M. Newville, P. Livins, Y. Yacoby, J.J. Rehr, E.A. Stern, Phys. Rev. B 47 (1993) 4126.
[23] J.J. Rehr, J. Mustre de Leon, S.I. Zabinsky, R.C. Abers, J. Am. Chem. Soc. 113 (1991) 5135.
[24] J.J. Rehr, J. Mustre de Leon, S.I. Zabinsky, R.C. Abers, Phys. Rev. B 44 (1991) 4146.